DNS, EXPERIMENTAL AND MODELLING STUDY OF AXIALLY COMPRESSED IN-CYLINDER SWIRLING FLOW

Jochen Volkert[1], **Henri Pascal**[1,3]
[1] Lehrstuhl für Strömungsmechanik, University of Erlangen, Cauerstrasse 4, 91058 Erlangen, Germany

Suad Jakirlić[2], **Cam Tropea**[2]
[2] Fachgebiet Strömungslehre und Aerodynamik, Darmstadt University of Technology, Petersenstrasse 30, 64287 Darmstadt, Germany

Kemal Hanjalić[3]
[3] Faculty of Applied Physics, Delft University of Technology, Lorentzweg 1, 2628 CJ Delft, The Netherlands

ABSTRACT

This paper reports on recent progress in the investigation and modelling of joint effects of compression and swirl on turbulence in a cylinder of a single-stroke rapid compression machine (RCM). Experimental and modelling investigation in a flat cylinder geometry, reported earlier (Hanjalić et al., 1997b), have been extended to cover a 'squish' configuration with a bowl in cylinder head and to broaden the range of operating conditions. In addition, the Direct Numerical Simulations (DNS) of all three operational modes of RCM have been performed: steady rotation and transient spin-down without and with compression. The Reynolds-Averaged Navier-Stokes simulation (RANS) were performed using the low-Re-number second-moment closure. The results obtained are compared with the experimental results (Volkert et al., 1996, 1998) and with DNS (Pascal, 1998). Prior to the computation of the RCM, the applied turbulence model was validated in several generic flows relevant to the RCM: developed and developing flows in an axially rotating pipe, swirling flows in combustion chamber geometries and long straight pipes (Jakirlić et al., 1998), as well as in several compression flow cases, ranging from homogeneous compression to the compression in a closed cylinder. It is demonstrated that in all cases considered the applied RANS model reproduces well both the DNS and experimental results.

INTRODUCTION

The main goal of the present study is to improve the RANS model(s) for predicting the flow in cylinders of IC engines. These flows are exceedingly complex, involving high swirl numbers, high degrees of anisotropy, compression effects and, in the case of fired engines, the interaction with the combustion process. Even restricting the attention to the isothermal case, large differences can be found between the predictions of the same flow using different codes and turbulence models - a situation which is highly unsatisfactory from the viewpoint of the engine developer.

In this paper we present some results of experimental and numerical investigations of the time-dependent, in-cylinder flow encountered in the rapid compression machine (RCM). The RCM, Fig. 1, consists of a transparent rotating cylinder head and stationary part accommodating a piston (Volkert et al., 1996, 1998). The rotating section, driven by an external motor, generates the flow rotation in the cylinder, providing thus a well defined initial state of the flow prior to the piston movement i.e. compression. In such a way both the compression and an initial swirl are imposed without a valve-generated inlet flow, which tends to induce complicating secondary currents. The intention of the experiment was to reduce the engine flow to a simple generic situation in which the effects of two major strain rates i.e. swirl and compression, can be studied free from contamination by other phenomena. Such well defined experimental results should serve as a basis for the validation of the RANS models.

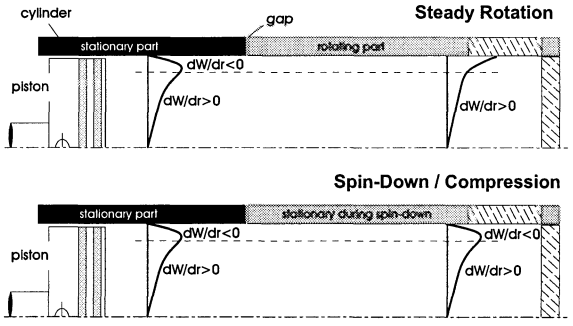

Figure 1: Design of the Rapid Compression Machine

In parallel to the experiments, the Direct Numerical Simulations (DNS) of all three operational modes of RCM were additionally performed, providing additional information which are not tractable to experimental techniques. A comprehensive data set was thus collected which enable a further insight in the effects of a single-stroke, anisotropic

compression and swirl on the evolution of turbulence, and provides a basis for comparison and validation of RANS models.

The following sections briefly describe the experimental and solution methods used. It will be followed by the results of some test cases accounting separately for rotating i.e. swirl and mean flow compression effects. Finally a selection of results for all three RCM cases will be presented.

EXPERIMENTAL METHOD

Experimental Apparatus - RCM. The experimental operation consists primarily of two phases. While the first phase is related to the generation of swirl inside the cylinder through cylinder rotation, an axial compression of the swirling flow is realized in the second phase.

As shown in Fig. 1, the apparatus consists of a rotating part (including the cylinder head), driven by an external DC motor, and a non-rotating part, both separated by a small gap ($\Delta z = 1mm$). The initial swirl intensity is controlled by the rotation rate of the cylinder, with experiments being performed at 30, 300, 1200 and 1800 rpm.

After stopping the cylinder rotation, an axial compression of the in-cylinder swirling flow is performed by a hydraulically driven piston. The compression ratio has been fixed to a value of $\epsilon_c = 5.0$. The compression (or strain) rate S, which is defined as the instantaneous piston speed $U_p(t)$ versus the length of the current volume to be compressed ($L(t)$),

$$S = \frac{1}{L(t)}\frac{dz_p}{dt} = \frac{U_p(t)}{L(t)}, \tag{1}$$

was variied in the range of $0.0 \leq S \leq 11.5\ s^{-1}$. Since the piston velocity can be controlled by the hydraulic system, an exponentially decaying velocity was used, corresponding to a constant strain rate during the entire compression stroke. Note that non-rotating section serves as acceleration length of the piston to its desired initial compression velocity when passing the gap. For optical access, the cylinder head is made out of glass.

Laser Doppler Anemometer (LDA). A four-beam, two-component backscatter LDA (5W Ar-Ion Laser, lambda=488/514,5 nm) with measurement volumes of $25.8\ \mu m$ and $27.2\ \mu m$ was used for velocity measurements. The scattered light was directed to color separation optics, directly connected to photomultipliers. After passing the signals through a two-channel downmixer and bandpass filters, counter processors (TSI 1990/1980) were used for signal processing. Oil droplets (mixture 1:1) with diameters of $d_P \leq 1\ \mu m$ were used for seeding, injected through the gap during the spin-up phase. Since the experiment is a one-shot experiment, all data acquisition was synchronized to the cylinder stop signal. Cycle-resolved averaging was performed with time domain filtering (spline smoothing) of the in-cycle velocity time series. Up to 200 repetitions were performed to build statistics about the flow field. Thus the mean velocity refers to the time mean velocity for steady rotation but to a phase mean velocity for all other measurements. Further details of the experimental facility can be found in the work of Volkert (1999).

MATHEMATICAL MODEL AND NUMERICAL METHOD

Both computational methods, the DNS and RANS were used for simulation of all three operational modes of the RCM:

- steady rotation of the cylinder i.e. generation of the initial swirl ($\partial/\partial t = 0$),
- spin-down (flow evolution after cylinder rotation is abruptly stopped) and
- spin-down with compression,

The continuity and Navier-Stokes equations governing the flow in the RCM take the following forms in the moving coordinate frame:

$$\frac{\partial}{\partial t}\int_V \rho dV + \int_S \rho(U_i - U_{bi})n_i dS = 0 \tag{2}$$

$$\frac{\partial}{\partial t}\int_V \rho U_i dV + \int_S \rho U_i(U_j - U_{bj})n_j dS = \int_S T_{ij}n_j dS \tag{3}$$

where U_{bi} stands for the velocity of moving boundaries of the computational domain. In the case of one-dimensional compression $U_{bi} = (U_P,\ 0,\ 0)$, where U_P represents the piston velocity. In the DNS code, a transformation of coordinates is used, while in the RANS finite volume code the *space conservation law* method (SCL, Demirdžić, Perić, 1990), is applied in order to conserve the number of mesh cells during the compression stroke. Details of the methods used can be found in Hanjalić et al. (1997b) for RANS, and in Pascal (1998) for DNS.

The stress tensor T_{ij} reads as follows:

$$T_{ij} = -P\delta_{ij} + \mu\left(\frac{\partial U_i}{\partial x_j} + \frac{\partial U_j}{\partial x_i}\right) - \frac{2}{3}\mu\frac{\partial U_k}{\partial x_k}\delta_{ij} \tag{4}$$

After the Reynolds decomposition of all instantaneous variables was applied ($U_i = \overline{U_i} + u_i$, $P = \overline{P} + p$), the stress tensor takes the following form in the framework of the RANS approach:

$$T_{ij} = -\overline{P}\delta_{ij} + \mu\left(\frac{\partial \overline{U_i}}{\partial x_j} + \frac{\partial \overline{U_j}}{\partial x_i}\right) - \frac{2}{3}\mu\frac{\partial \overline{U_k}}{\partial x_k}\delta_{ij} - \rho\overline{u_i u_j} \tag{5}$$

The Reynolds stress tensor $-\rho\overline{u_i u_j}$ is to be defined by an appropriate turbulence model.

Simulations by both methods were performed in a cylindrical inertial frame of reference involving all three velocity components and six Reynolds stress components. The axisymmetric approximation ($\partial/\partial\varphi = 0$) was applied for all RANS computations, simplifying to a large degree the computational effort.

Assuming that acoustic waves have an insignificant effect on the turbulence (e.g. Wu et al., 1985), the fluctuating field is viewed as incompressible ($\partial u_i/\partial x_i = 0$), interacting with a compressible mean flow. Therefore the gas density is only a function of time and temperature. The time variation of viscosity is accounted for by Sutherland's law. For adiabatic compression these relations are:

$$\left[\frac{\rho(t)}{\rho_o}\right]^{\kappa-1} = \frac{T(t)}{T_o}\ ;\ \ \frac{\mu(t)}{\mu_o} = \left[\frac{T(t)}{T_o}\right]^{0.75} \tag{6}$$

where in both equations (6) the index "o" refers to the beginning of the compression process. The homogeneous density also implies a homogeneous divergence of the mean velocity so that the terms in Eq. (3) representing molecular momentum transport are free of dilatational effects.

Without further elaboration, it can be stated that simple eddy-viscosity models can not capture essential features of this flow, in which swirl and compression effects lead to

strong anisotropy of both the stress and dissipation tensors. The same statement stands also for the use of wall functions. As an illustration, Fig. 2 presents measured and computed near-wall profiles of the tangential and axial velocity for the spin-down cases without and with compression.

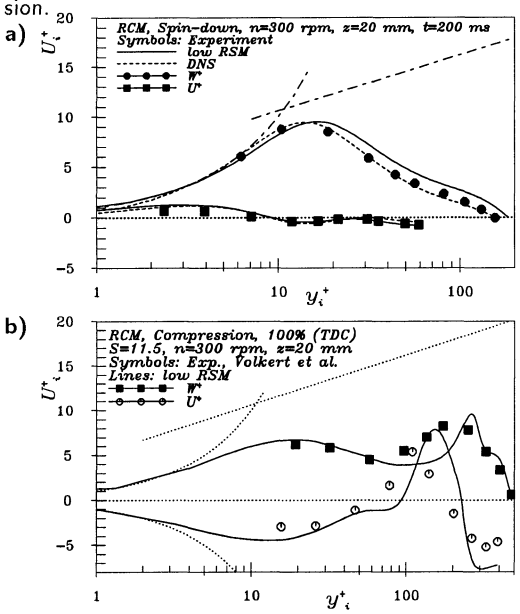

Figure 2: Departure of the mean axial and the mean tangential velocities from the logarithmic law: spin down without (a) and with compression (b)

Clearly, there is a dramatic departure from the equilibrium linear and logarithmic mean velocity distribution, illustrating the necessity to integrate governing equations up to the wall. For these reasons, the numerical simulations were performed using a low-Re Reynolds-stress model, based on the standard high-Re-number $\overline{u_i u_j} - \varepsilon$ closure (Gibson, Launder, 1978), which serves as high-Re-number asymptote, Hanjalić et al., 1997a, 1999). The model contains modifications which account for the low-Re-number and non-viscous wall blockage effects, as well as pressure reflection in terms of invariant local turbulence parameters, such as invariants of the anisotropy of Reynolds-stress and dissipation-rate tensors, as well as turbulence Reynolds number. In addition to satisfying most of the basic physical constraints, the model was shown to reproduce very well the mean flow and turbulence properties - particularly in the vicinity of a solid wall - in a broad variety of non-equilibrium flows featuring different phenomena. The validation cases include a series of attached and separating flows with strong time- or space-variations, or abrupt changes of boundary conditions in a wide range of Re-numbers.

In addition to the computations by the low-Re Reynolds-stress model described, for comparison most flow cases considered were also computed by other models, which are most widely used in industrial applications. These include several two-equation models and several Reynolds-stress models, with application of both kinds of the wall boundary conditions: the exact ones (low Re models) and wall functions.

RESULTS OF THE FLOW SIMULATIONS

Before presenting results for the major test case (simultaneous swirl and compression), we consider first several examples in which only one of the effects was present.

Rotating and Swirling Flows

Several types of rotating and swirling flows have been studied aimed at analyzing the vortex dynamics and identifying some features which pose a special challenge to the turbulence modelling. The flows considered cover a range of situations which may not be directly relevant to engine flows, but enable in depth analysis of the flow phenomena associated with rotation and swirl: the developing and fully developed flows in an axially rotating pipe (a steady rotation mode), swirling flows in combustor geometries and long pipes (related to the spin-down mode, i.e. to the decay of the swirling motion) and several homogeneous flows subjected to rotation, but with some additional straining. For brevity, only some aspects will be here considered.

Generally, all computational results for swirling flows entering the pipe/cylinder geometries are in reasonable agreement with available experimental data. Some shortcomings have been noted in reproducing specific features such as, e.g. the $\overline{uw}$-anomaly, capturing the transition from a concentrated vortex type of the mean swirl velocity to the solid body rotation in a long straight pipe with a weak swirl, underprediction of the normal stress components in the core region and a premature flow laminarization in rotating pipes/cylinders, but these deficiencies do not seem to affect much the satisfactory reproduction of major mean flow and turbulence parameters (Jakirlić et al., 1998). As an illustration, the comparison between experimental (Steenbergen, 1995) and modelling results of the Reynolds stress components at a selected position in the swirling flow in a long straight pipe is shown in Fig. 3.

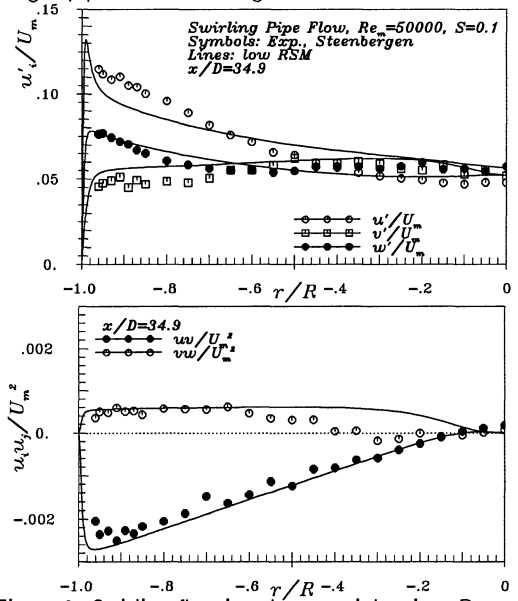

Figure 3: Swirling flow in a long straight pipe: Reynolds stress components

Compressed Flows

Several cases of homogeneous compression (Wu et al., 1985; Le Penven, Serre, 1993) were investigated before considering the compression in a closed piston/cylinder assemblies. These computations were aimed at investigat-

ing the applicability of some popular second-moment closures (LRR, SSG, Fu-Launder-Tselepidakis, Shih-Lumley, Launder-Tselepidakis) and the present model, under the influence of the mean flow compression. The time behaviour of the turbulence kinetic energy was reproduced reasonably well by all models applied.

A single-stroke compression in a closed cylinder with a sinusoidal variation of the piston velocity was then investigated in parallel by both the RANS approach and DNS. Fig. 4a shows the mean axial velocities at four selected times during a compression stroke. The compression ratio ($\epsilon_c = L_o/L_{TDC} = 4.2$) is almost identical to that investigated experimentally and with DNS in the RCM ($\epsilon_c = 5.0$). The value of rapidity: Sk/ε ($S = \partial U_z(t)/\partial z(t) = 1/\rho\partial\rho/\partial t$) is very close to that found in real IC engines ($\approx 2-3$). The mean velocities obtained by HJ low-Re second moment closure are compared with the results of DNS performed by Pascal, 1998 (this flow was simulated earlier by Güntsch and Friedrich, 1996, also by DNS). The low-Re-number model applied here, reproduces well the onset of separation at the crank angle of about 138° and the near-wall velocity field, though it fails to capture the DNS peak in the velocity profile. It is noted that the application of the wall functions fails to capture the near-wall behaviour and , consequently, can not reproduce the separation in accord with DNS findings.

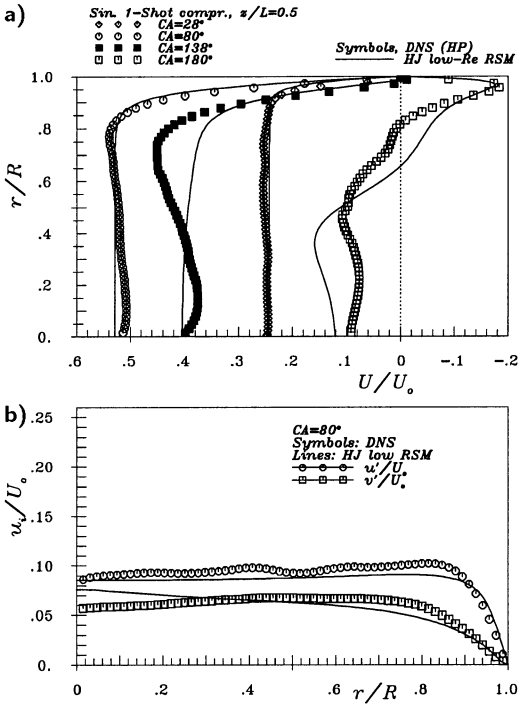

Figure 4: 1-shot sinusoidal compression in a closed cylinder: mean velocities and turbulence intensities

Fig. 4b shows the streamwise and normal-to-the-wall stress components at 80°. The intensity of both stress components as well as their near wall behaviour are in good agreement with the DNS data.

Flow cases in the RCM

A selection of experimental and numerical results of the steady rotation as well as spin-down flow cases without and with compression is shown in the following figures.

Steady rotation. As already said, the steady rotation operational mode serves for the generation of the swirl motion which is then compressed by the piston movement. In this phase the flow is driven by rotation of cylinder walls and the weak fluid movement in $r-z$ plane caused by the existence of the non-rotating cylinder part accommodating a piston. Fig. 5 shows experimentally and numerically obtained axial velocity profiles for the steady rotation mode both for flat and bowl configuration of the RCM.

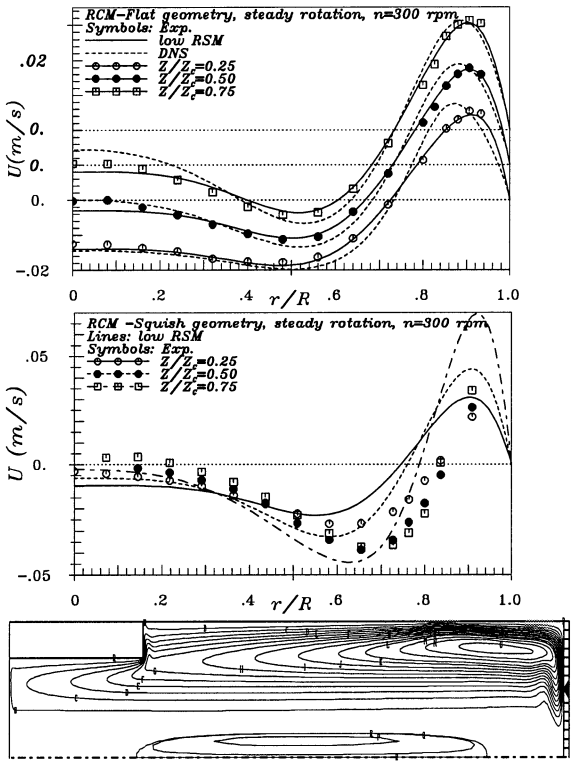

Figure 5: Steady Rotation: axially velocity profiles for flat (upper) and bowl (middle) configuration and streamlines computed by HJ low-Re RSM (lower)

The basic shape of the profiles for both geometries are similar. However, close to the cylinder axis, a second change in the sign of the axial velocity at Z/Z_c=0.75 in the bowl geometry obtained experimentally indicates the existence of a free stagnation point. The appearance of 'floating' vortices in fast rotating flows has been reported by a number of authors and with these investigations we hope to contribute to further enlightenment on this phenomenon. The streamlines plot obtained by the model computations confirms clearly the existence of such a swimming vortex. Compared to the available experimental results this computationally obtained bubble is obviously shifted towards the interior of the RCM. Whereas a very weak dependency of axial direction was documented for the flat geometry, a noticeable streamwise velocity gradient is observed in bowl configuration, indicating an enhancement of the (secondary) motion in the $r-z$ plane.

Spin-down flow cases. Fig. 6 shows in parallel the

RANS and DNS streamline patterns (computed from mean axial and radial velocity components) for two time positions during the spin down without compression: at the very beginning of the spin-down (corresponding to the steady rotation mode) and at a later stage. Both, the DNS and model computations confirm the existence of a large vortex in the r-z plane. The vortex breaks up after the cylinder rotation is stopped approximately at $t = 200ms$, generating two counter rotating vortices. After stopping of the endplate rotation, the driving force of the secondary motion imposed by the centrifugal acceleration of fluid due to tangential motion close to the rotating endplate, disappears. A boundary layer develops at the static endplate, propagating axially into the cylinder. Therefore, the region of maximum outward radial momentum moves away, creating an interface between the two vortex structures.

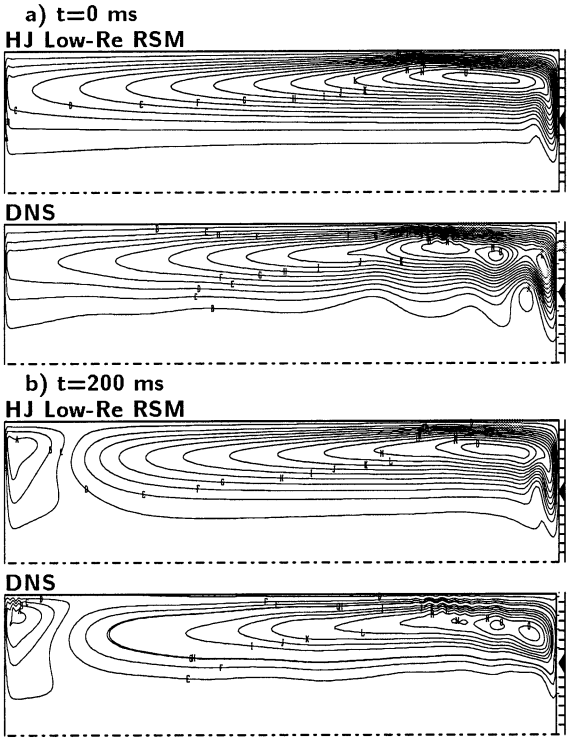

Figure 6: Streamlines computed by HJ low-Re RSM and DNS for two selected times during the spin-down operational mode of RCM

Such a behaviour is in accordance with the change of the sign of the tangential velocity gradient, i.e. the Richardson number, from positive (steady rotation mode) to negative (spin down-mode). This vortex splitting, as well as the consequent change of the mean velocity sign, is detected also by experiment, Fig. 7.

Fig. 8. shows both the experimental and numerical results of the mean tangential velocity profiles as well as computationally obtained velocity vectors in the r-z plane at two selected time positions during the compression stroke. The boundary layer developing on the cylinder wall is separated due to the piston movement, creating ring shaped eddies. The increasing compression causes a convection of these eddies towards the core region, creating smaller eddies, which leads eventually to a complex flow structure.

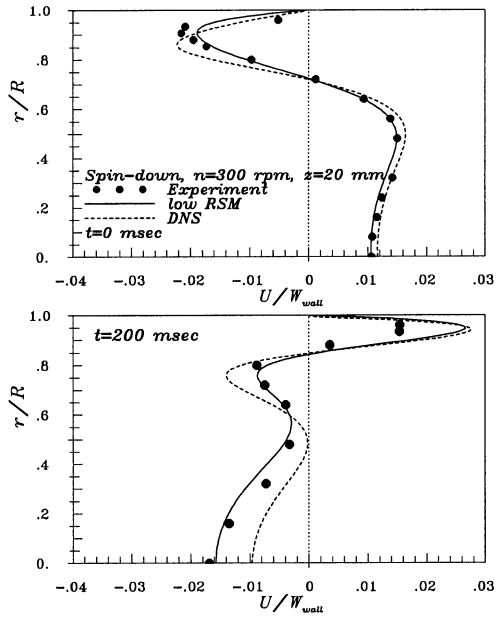

Figure 7: Evolution of the axial mean velocity profile during the spin-down operational mode of RCM

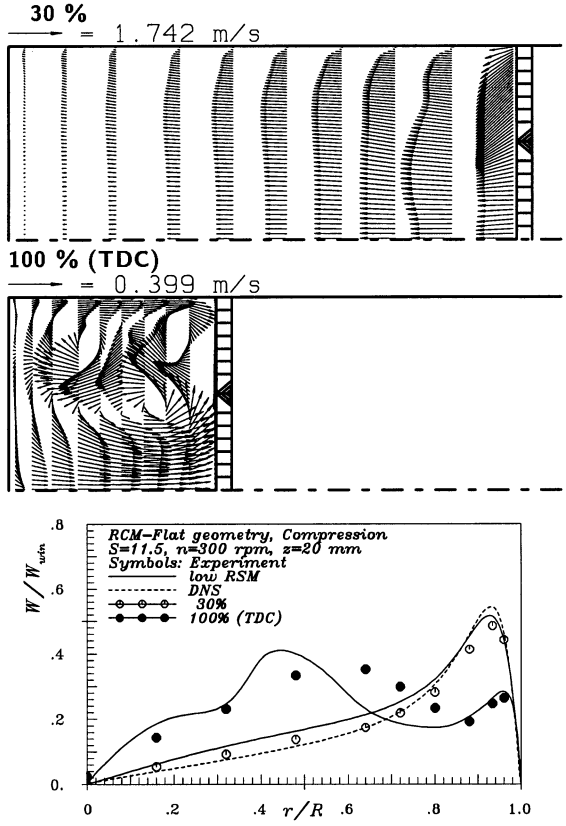

Figure 8: Velocity vector plots and tangential mean velocity profiles at two selected time positions during a compression stroke

The computed axial velocities deviate substantially from the experimental profiles (not shown here). The most likely reason is that both the RANS and DNS did not account

for the gap between the rotating and non-rotating cylinder parts, which is unavoidable in the experiment for a frictionless cylinder rotation as well as for the particle seeding, Fig. 1. It is noted that despite the deviation mentioned, agreement between the tangential velocities for these and all other time positions is very good. The tangential velocity shows that the initial wall-jet type velocity profile becomes strongly deformed by compression. This process starts at about 30% of the compression stroke.

The deformation of the velocity field is further illustrated in Fig. 9 where the time evolution of the tangential velocity is shown for two radial positions. The characteristic modifications of the tangential velocities, observed by experiment, are reasonably well captured by the model computations. The effect of compression on the mean velocity field and the ability of the model to reproduce this effect in accord with DNS results is also well illustrated in Fig. 2., showing very different shapes of both the axial and tangential velocity profiles in the spin-down mode without (Fig.2a) and with compression (Fig. 2b).

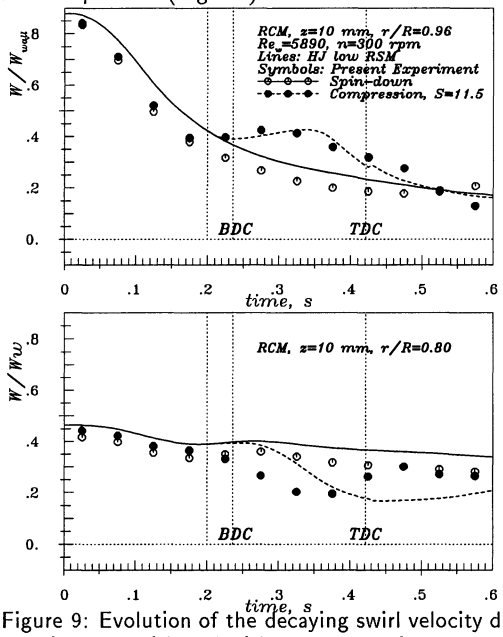

Figure 9: Evolution of the decaying swirl velocity during the spin-down with and without compression - comparison with experiment

CONCLUSIONS

The combined experimental and numerical (DNS plus RANS) investigations of the flow and turbulence in the piston-cylinder configuration pertinent to IC engines were conducted by considering a single-stroke rapid compression machine (RCM) in which an initially homogeneous turbulence was subjected separately and simultaneously to swirl and compression. These investigations were aimed at analyzing the potential of the single-point turbulence closure for prediction of flow aerodynamics in cylinders of IC engines. The basis for the analysis are the experiments and DNS, which were performed in parallel for the same configuration. They showed that the simultaneous action of swirl and compression produces a complex flow pattern with a dual eddy structure as a consequence of vortex break-up. The flow separates at the wall at a certain crank angle and the stress field becomes highly anisotropic. Application of some popular eddy-viscosity and Re-stress models showed that only the latter models have a potential for capturing the complex flow features, but require the integration up to the wall. It is further shown that the low-Re-number second-moment closure, developed earlier and validated in a range of non-equilibrium flows (Hanjalić et al., 1997a, 1999), reproduces reasonably well most of the mean flow and turbulence features in all three cases considered. Some interesting details are discussed in light of the DNS evidence on the effects of flow rotation and compression.

Acknowledgement. This work was sponsored by the EC JOULE III Programme, Contract JOF3-CT95-0017 and DFG, Contract Tr 194/7.

REFERENCES

Demirdžić, I., Perić, M. (1990): "Finite volume method for prediction of fluid flow in arbitrarily shaped domains with moving boundaries," *Int. J. for Numerical Methods in Fluids*, Vol. 10, pp 771-790

Güntsch, E., Friedrich, R. (1995): "Compression of initially isotropic turbulence in a cylinder at low Reynolds number," *10th Symposium on Turbulent Shear Flows*, The Pennsylvania State University, USA

Hanjalić K., Jakirlić S., Hadžić I. (1997a): "Expanding the limits of "equilibrium" second-moment turbulence closures," *Fluid Dynamics Research*, Vol. 20, pp 25-41

Hanjalić K., Jakirlić S., Keller, J., Tropea, C., Volkert, J. (1997b): "Evolution of cylinder spin-down turbulence subjected to a single-stroke compression: experiments and modelling," *11th Symp. on Turbulent Shear Flows*, Grenoble, France

Hanjalić, K., Hadžić, I., Jakirlić, S. (1999): "Modelling the turbulent wall flows subjected to strong pressure variations," *ASME J. of Fluids Eng.*, Vol. 121(1), pp 57-64

Jakirlić S., Hanjalić K., Tropea C., Volkert J. (1998): "On the computation of rotating and swirling confined flows with second-moment closure models," *7th Symp. on Flow Modelling and Turbulence Measurements*, Tainan, Taiwan

Le Penven L., Serre G. (1993): "Homogeneous turbulence submitted to compression: experimental study and modelling," *9th Symp. on Turbulent Shear Flows*, Kyoto, Japan

Keller, J., Volkert J., Tropea C. (1998): "Influence of Axial Compression on a Strongly Swirling Cylinder Flow," *9th Int. Symp. on Applications of Laser Techniques to Fluid Mechanics*, Lisbon, Portugal

Pascal, H. (1998): "Numerical Simulation for the Study of Internal Combustion Engines Flows," LSTM Report, University Erlangen-Nuremberg, Germany

Steenbergen, W. (1995): "Turbulent Pipe Flow with Swirl," PhD Thesis, Eindhoven University

Volkert J., Tropea C., Domann R., Hübner W. (1996): "Combined Application of PIV and LDA to Swirling Flows under Compression," *8th Int. Symp. on Applications of Laser Techniques to Fluid Mechanics*, Lisbon, Portugal

Volkert J. (1999): "Experimentelle und numerische Studie komprimierter Drallströmungen," Ph.D. Thesis, University Erlangen-Nuremberg (in German)

Wu C.T., Ferziger J.H., Chapman D.R. (1985): "Simulation and modelling of homogeneous, compressed turbulence," *5th Symp. on Turbulent Shear Flows*, Ithaca, NY